Exploring the Temperature and Composition Dependence of the Ionic Transport in Solid-State Battery Composites

Yannik Rudel,[1] Marvin A. Kraft,[2] Lukas Ketter,[1,3] and Wolfgang G. Zeier[1,2,3,*]

[1] *Institute of Inorganic and Analytical Chemistry, University of Münster, Corrensstrasse 28/30, 48149 Münster, Germany*

[2] *Institut für Energie- und Klimaforschung (IEK), IEK-12: Helmholtz-Institut Münster, Forschungszentrum Jülich, Corrensstrasse 46, Münster 48149, Germany*

[3] *International Graduate School of Battery Chemistry, Characterization, Analysis, Recycling and Application (BACCARA), University of Münster, 48149 Münster, Germany*

(Received 5 June 2024; accepted 12 August 2024; published 30 August 2024)

Solid-state electrolytes offer a promising avenue for energy storage in the context of lithium-based batteries, not only from an energy density perspective, but also by eliminating issues such as freezing of the liquid electrolyte at low temperatures and the performance limitations associated with that. In solid-state batteries, solid electrolytes are not only used in separators but are also needed in composite electrodes. However, the transport properties of solid-state battery composites are often investigated at room temperature, while the temperature dependence of effective ion transport as a function of volume fraction remains underexplored. Therefore, this work investigates the effective ionic transport in composites of multiple sulfide-based solid electrolytes with Si/C as the active material, as a function of composition and temperature. Analyzing impedance spectra with a transmission line model, this work reveals changes in activation barrier and with that the temperature dependence of ion transport upon varying the volume ratios. This finding emphasizes the importance of considering the activation energy in solid-state battery design to tailor battery performance to the temperature range of application.

DOI: 10.1103/PRXEnergy.3.033004

I. INTRODUCTION

Advancements in battery technology are essential for enabling the widespread adoption of electric vehicles, as this sector of battery application is set to grow rapidly in the foreseeable future [1]. The temperature limitations associated with traditional liquid electrolytes have become apparent, and issues such as freezing of the liquid electrolyte at low temperatures, and thus, sudden reduction in conductivity, have prompted the need for new solutions to improve battery performance [2]. One promising solution to overcome the drawbacks of liquid electrolytes is the implementation of solid-state electrolytes. Unlike their liquid counterparts, solid electrolytes eliminate the risk of sudden drops in conductivity, as they are already solid and show Arrhenius-like behavior over a wider range of temperature [3]. The implications of this hold significant meaning for real-world applications, particularly in the context of enhancing the efficiency and reliability of batteries in diverse environmental conditions. The choice of anode material is another crucial aspect influencing battery performance. As the dense lithium metal anode in solid-state batteries exhibits performance limitations at low temperatures, other common active materials like graphite or high-capacity alternatives like silicon are being considered as substitutes [4,5]. While some dense silicon anodes have shown promising performances, their areal loading remains limited, which is why Si-based solid-state composite anodes are most often explored. Their cycling stability, however, suffers more dramatically from volume changes upon delithiation or lithiation [6–8]. This work employs a silicon on graphite (Si/C) composite material with a graphite content of 92–93 wt %, which addresses the volume expansion concerns, as carbon not only functions as an active material but also acts as a buffer for volume expansion [9]. This Si/C composite was employed before, it was shown that larger solid electrolyte volume fractions led to better solid-state battery performance due to faster lithium ion transport in the composite [10]. Additionally, Rana *et al.* investigated the dependence of silicon-based

*Contact author: wzeier@uni-muenster.de

composites on the size of active material particles and the ionic conductivity of the chosen electrolyte, indicating that a faster electrolyte and smaller active material particles led to improved electrochemical performance [11].

The temperature-dependent performance of solid-state batteries has been explored in the past. For instance, Kato *et al.* showed that thick electrode setups could adequately perform at room temperature, if the tortuosity factor was sufficiently low or the lithium ion conductivity of the solid electrolyte was sufficiently high [12]. Some information on the conductivity dependence of the low-temperature performance was provided by Peng *et al.* [13] by employing $Li_{5.5}PS_{4.5}Cl_{1.5}$ at room temperature and −20 °C at various *C* rates over up to 200 cycles. They showed that the fast-conducting solid electrolyte could enable an adequate low-temperature performance for solid-state batteries, however at a limited cathode active material loading of 2.5 mg cm^{-2}. More extensive temperature studies on multiple solid-state battery architectures were performed by Lu *et al.* [14], showing that degradation or passivating layers might limit the low-temperature performance of solid-state composite cathodes. However, avoiding those cathode limitations results in promising low-temperature performances, down to even −40 °C, facilitated by low active material loadings (3.8 mg cm^{-2}) and a highly conductive solid electrolyte (∼10 mS cm^{-1}). For these temperature-dependent investigations, the composition of the composites was also pushed towards high solid electrolyte and carbon additive contents; this was linked to effective transport in solid-state electrodes, a recently more widely discussed topic. Dewald *et al.* [15] and Minnmann *et al.* [16] were able to show that balancing volume fractions, and thus, the electronic and ionic conductivity in cathode composites, was crucial for optimal performance. Hendriks *et al.* also showed this to be true for $LiMnO_2/Li_3InCl_6$ composites [17]. Zhang *et al.* gave insights into the composition dependence of $LiCoO_2$-based composites by showing that the capacity and cyclability of these composites was majorly influenced by their composition [18]. Additionally, Naik *et al.* investigated cathode performance in relation the active material content, giving insights into the relationship between electrode thickness and current density dependence of solid-state electrodes. They were able to show that a carbon binder as a secondary phase might not be beneficial for cell performance by giving preferred regimes of active material and carbon content in relation to electrode capacity [19]. Furthermore, Zahnow *et al.* investigated the impact of porosity in NCM ($LiNi_{1/3}Co_{1/3}Mn_{1/3}O_2$) cathode material on the electronic and ionic conductivity, showing nontrivial behavior of the effective conductivities and corresponding activation energies [20].

With the temperature and composition dependence of ion transport in electrode composites investigated, their interdependence, i.e., parallel examination of both, remains underexplored. Therefore, in this work, the ionic conductivities of electrode composites are investigated as a function of Si/C to solid electrolyte (SE = Li_6PS_5Cl, $Li_{5.5}PS_{4.5}Cl_{1.5}$, and Li_6PS_5Br) volume ratio and temperature by impedance analyses with a transmission line model (TLM). This work shows that changes in volume fractions (ϕ) of the active material lead to changes in the activation energy for ionic transport in composites. The faster increase in impedances at lower temperatures for high volume fractions of active material shows that the focus in solid electrolyte research should not only be to find high ionic conductivities at room temperature, but also to find as low activation barriers as possible to achieve stable solid-state battery performance across a wide range of temperatures. It further shows that, for low-temperature operation, lower active material loadings may be necessary if much faster solid electrolytes cannot be developed.

II. EXPERIMENTAL SECTION

A. Electrolyte preparation and characterization

All materials and samples were handled under an argon atmosphere [$p(O_2) \leq 0.1$ ppm, $p(H_2O) \leq 3$ ppm]. The solid electrolytes Li_6PS_5Cl, $Li_{5.5}PS_{4.5}Cl_{1.5}$, and Li_6PS_5Br were prepared in 3 g batches using the precursors Li_2S (Alfa-Aesar, 99.9%), LiCl (Alfa-Aesar, 99%), LiBr (Alfa-Aesar, 99.99%), and P_2S_5 (Sigma-Aldrich 99%) in stoichiometric ratios mixed in an agate mortar and homogenized by manual grinding for 15 min. Afterwards, the powder was hand-pressed into pellets ($d = 10$ mm) and transferred to predried (dynamic vacuum at 800 °C for 2 h) and carbon-coated quartz glass ampoules. The ampoules were sealed under vacuum and annealed in a tube furnace at 550 °C for 14 days in the case of Li_6PS_5Cl and Li_6PS_5Br. $Li_{5.5}PS_{4.5}Cl_{1.5}$ was annealed at 450 °C for 3 days twice, with intermediate regrinding and subsequent pelletizing as described. All products were hand-ground in an agate mortar for further use and characterization. The purity of the solid electrolytes was confirmed by x-ray powder diffraction of the samples sealed in borosilicate glass capillaries that were spinning during data collection [Stoe STADI P, $2\theta = 10°$–$80°$, λ(Cu $K\alpha 1$) = 1.54 Å, with a DECTRIS MYTHEN 1 K detector] (Fig. S1 within the Supplemental Material) [21].

B. Composite preparation

Composites of the synthesized solid electrolytes and Si/C particles were prepared with different nominal volumetric ratios targeting 30, 40, and 50 vol% solid electrolyte contents. The equivalent weight ratios were calculated using the respective densities (Table SI within the Supplemental Material [21]). Mixing was performed in 200 mg batches for 15 min using a mini shaker mill (Fritsch, PULVERISETTE 23) in a 15 ml ZrO_2 cup using

15 ZrO_2 balls (Ø = 3 mm) at 45 Hz. The Si/C composite material is described elsewhere [22].

C. Cell assembly and electrochemical measurements

All cells were assembled in a custom-made PEEK cylinder with an inner diameter of 10 mm surrounded by a brass casing. Stainless-steel stamps were employed for pressing and current collectors [18]. Before any measurements were conducted, the cells were held under pressure (50 MPa) for 5 h to ensure equilibrated pressure in the cell [23]. Cells for potentiostatic impedance spectroscopy of pristine solid electrolytes were prepared with 200 mg of only the respective argyrodite-type solid electrolyte. Cells for the determination of effective ionic transport properties in the composites using the TLM were prepared by first adding 80 mg of Li_6PS_5Cl as a separator into the cell and prepressing using a manual screw press, followed by adding 20 mg of the respective composite to each side of the separator.

Potentiostatic electrochemical impedance measurements of the pristine argyrodites and the symmetric cells for transmission line modeling were performed at temperatures between −40 °C and 60 °C using a BioLogic SP-300 potentiostat (7 MHz–50 mHz, 15 points per decade, excitation voltage = 10 mV). The temperature was increased in 10 °C increments, with additional room-temperature steps prior to and after the temperature ramp as well as in between the 20 °C and 30 °C steps. After temperature stabilization, a 2 h waiting period before collecting impedance spectra was used to ensure that the whole cell had equilibrated to the desired temperature. In this work, we applied transmission line modeling to the potentiostatic impedance spectra of the electron blocking cells to determine the effective ionic conductivity within the prepared composites. Cells for validation by direct current measurements were prepared by adding 80 mg of Li_6PS_5Cl, 10 mg of the composite (50 vol % Li_6PS_5Cl and 50 vol % Si/C), and another 80 mg of Li_6PS_5Cl followed by handpressing after each step. After assembly, all cells were pressed in a uniaxial press at a pressure of 374 MPa for 3 min. Onto those cells (only for direct current measurements), an indium (chemPUR, 100 µm thickness, 99.99%) disk (9 mm, 50 mg) followed by a freshly pressed lithium (abcr, 99.8%) disk (4 mm, 1.5 mg) were added to both sides of the cell. Each such cell assembly was put into an aluminum frame and pressure was applied by a screw with a torque of 10 Nm (50 MPa) during electrochemical measurements [18]. Polarization measurements using a direct current were conducted to determine the effective ionic conductivities using a Metrohm AutoLab potentiostat (PGSTAT302N). Before the measurement was started, an equilibration time of 6 h was set. This time was also used to equilibrate the temperature, as new cells were built for each temperature. Applied voltages of 2.5, 5, 7.5, 10, 15, 20, and 25 mV were each maintained for 3 h to allow the current to stabilize. A 1 h resting period was set between different voltage steps to ensure cell equilibrium. This measurement was performed at five different temperatures (5, 15, 25, 40, and 60 °C).

III. RESULTS AND DISCUSSION

A. Transport determination and model validation

Impedance spectroscopy allowed to quickly investigate temperature-dependent ionic conductivities when suitable equivalent circuit models are available and validated to describe the investigated processes. The determination of the ionic conductivities of pristine solid electrolytes is a well-established procedure that involves fitting the acquired impedance spectra while only considering the total ion transport (see Fig. S2 within the Supplemental Material) [21]. In the case of the effective ionic conductivity within the respective composites, this is complicated by the additional impedance response from electronically conductive carbon in the composites. In this case, a TLM can be employed to fit the impedance spectra of a symmetric cell setup (composite|solid electrolyte|composite), obtaining the ionic resistance of the composite. Due to the capabilities of extracting transport parameters, transmission line modeling of the electrode composite impedance spectra is used frequently, for instance, in NCM622-SE composites by Minnmann *et al.* [16] and Schlautmann *et al.* [24], $LiMn_2O_4$-SE composites by Hendriks *et al.* [17], as well as silicon-carbon-SE composites by Rana *et al.* [11]. Furthermore, Ohno *et al.* [25] and König *et al.* [26] successfully employed transmission line modeling to investigate carbon-SE systems applicable to sulfur solid-state cathodes and ionic transport in wet-milled NCM-$Li_{5.3}PS_{4.3}ClBr_{0.7}$ composites. A TLM study on the tortuosity of battery electrodes by Landesfeind *et al.* [27] shows that the TLM can successfully be employed for solid-state composites and that the tortuosity factor in these composites is significantly higher than the prediction made by Bruggemann Cronau *et al.* for instance, who have used the TLM for a thickness-dependent impedance study of $LiCoO_2$ cathodes in a liquid electrolyte system, which are generally well understood with transmission line modeling, showing that tortuosity factors are virtually independent of electrode thickness between 44 and 251 µm [28]. Additionally, it is standard practice to investigate solid oxide fuel cells using the TLM. A three channel TLM was used to model the different loss contributions in anode functional layers and showed that a thin substrate with high porosity was beneficial for performance [29]. Furthermore, it was shown that a three channel TLM for double-layered cermet anodes in solid oxide fuel cells offered enhanced accuracy and versatility in simulating anode performance, outperforming the two channel TLM in this case, and showed that optimizing the electrolyte

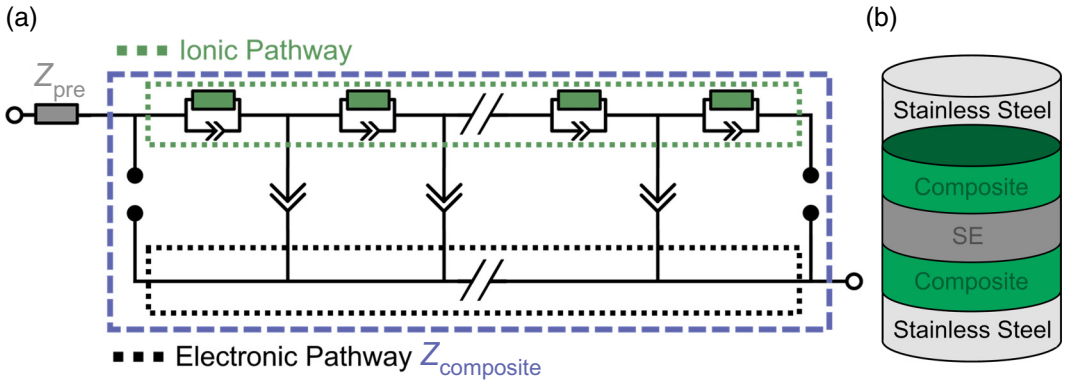

FIG. 1. (a) Employed TLM to determine the effective ionic conductivities of the composites. Impedance response of the composite is modeled by $Z_{composite}$. While the ionic pathway is highlighted in the dashed green line, the electronic pathway, modeled as a short circuit, is highlighted within the dashed black line. Resistance of the Li_6PS_5Cl separator is given by resistance Z_{pre}. (b) Schematic of the cell setup used for impedance measurements.

matrix materials for higher conductivity could significantly improve the performance of the anode layer [30].

The TLM used in this work is shown in Fig. 1(a) [also see Eq. (S1) and Fig. S3 within the Supplemental Material [21]]. In previous work, it was shown that the effective electronic conductivity of the Si/C:Li_6PS_5Cl-composite remained independent of the solid electrolyte content in the range of 0 to 50 vol %. Additionally, the effective electronic conductivity ($\sim$2.5 S cm^{-1}) is 4 orders of magnitude higher than the best ion conducting composite at room temperature [10]. Therefore, and due to the similarity of the different solid electrolytes employed, Li_6PS_5Br and $Li_{5.5}PS_{4.5}Cl_{1.5}$ compared with Li_6PS_5Cl, electronic transport is assumed to remain comparably high within all composites prepared. This assumption enables the electronic pathway in the TLM to be well described by a short circuit (i.e., negligible resistances). The impedance spectra show a high-frequency (3 kHz, apex frequency) process that can only be resolved for low temperatures (-40 to 0 °C). This process can be attributed to ion transport within the solid electrolyte separator, in accordance with the resistivity and capacitance of the pristine solid electrolytes. In Fig. S3(a) within the Supplemental Material [21], an exemplary fit of the low-temperature impedance spectra, also including the high-frequency process, is given with the respective equivalent circuit [Fig. S3(c) within the Supplemental Material [21]], confirming that this process can only be attributed to the separator. By excluding high-frequency responses originating from the separator, it was possible to account for these contributions with a simple resistor and use the same equivalent circuit to analyze all composite impedances throughout this work. Relevant equations for the TLM can be found in the Supplemental Material [21]. The capacitances of the ionic pathway are in the range of 10^{-6} F. While these are not in the range of bulk capacitances reported for solid electrolytes [31,32], at this stage, one may assume the measurement of an average over different processes, for instance, additional constriction resistances in the composite and artifacts originating from contacting, which explain the measured range [33,34].

The conductivity data gathered using this TLM were exemplarily verified for the composite containing 50 vol % Li_6PS_5Cl. This was done by building symmetric cells for direct current polarization measurements to determine the effective ionic transport at five different temperatures, similar to a previous report [10]. This comparison, as well as the schematic cell setup utilized, can be found in Fig. S3(b) within the Supplemental Material [21]. The comparability of the conductivities from direct current polarization to those obtained from transmission line modeling impedance spectroscopy confirm the validity of the TLM used.

B. Temperature behavior of effective ion transport

Figure 2 shows two exemplary impedance spectra of the composites containing 50 vol % Li_6PS_5Cl, $Li_{5.5}PS_{4.5}Cl_{1.5}$, and Li_6PS_5Br at -40 °C [Fig. 2(a)] and 25 °C [Fig. 2(b)] and the respective fitting curves from the TLM. Besides availability and general interest for application in solid-state batteries, these specific solid electrolytes were chosen since Li_6PS_5Cl and $Li_{5.5}PS_{4.5}Cl_{1.5}$ had similar activation energies, while $Li_{5.5}PS_{4.5}Cl_{1.5}$ had a significantly higher ionic conductivity [3,35]. Li_6PS_5Br was chosen as a material with a lower activation energy compared to the Cl-based electrolytes, while still being in the same argyrodite electrolyte family and conductivity range as Li_6PS_5Cl [3]. When only 30 vol % solid electrolyte was contained in the composites, fitting became unreliable at low temperatures (-30 and -40 °C) for Cl-rich argyrodite composites and at 60 °C for the Li_6PS_5Cl composite, as indicated by large uncertainties associated with the fitted parameters. However, trends within intermediate temperatures can still be

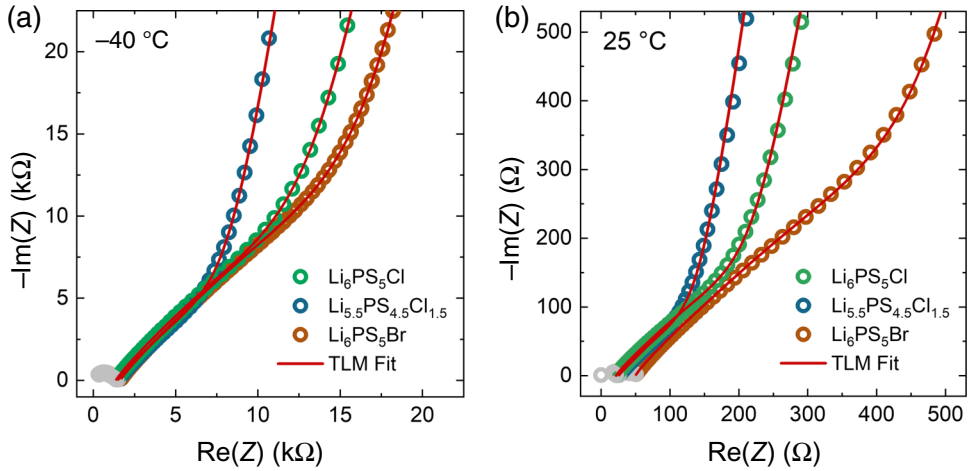

FIG. 2. Exemplary impedance spectra of the 50 vol % composites at −40 °C (a) and 25 °C (b) with the respective transmission line modeling in red. Data points of the frequency range excluded from fitting are shown in gray.

assessed, despite these limitations of modeling at extreme temperatures at lower volume percentages.

For all investigated composites, the effective ionic room-temperature conductivity ($\sigma_{\mathrm{eff,ion,RT}}$) scales with the amount of solid electrolyte in the composite [Fig. 3(a)]. In addition, similarly pronounced changes in the effective ionic conductivity are observed as a function of temperature (Fig. S4 within the Supplemental Material [21]). All composites show temperature-modified Arrhenius behavior in the change of the effective ionic conductivity with varying temperature, as also typically observed in the pure solid electrolytes. An exemplary Arrhenius-type plot of the temperature-dependent effective conductivities in composites containing Li_6PS_5Cl, showcasing the expected linearity, is given in Fig. 3(b). All Nyquist plots and respective fits for temperature-dependent conductivities (Figs. S6–S14) as well as Arrhenius plots (Fig. S5) are shown in the Supplemental Material [21]. As all composites show Arrhenius behavior of the effective ionic conductivity over the investigated temperature range, the activation energies can be calculated from the slope of a linear fit to the respective data [Fig. 3(b)]. The observed activation energies are given for the pristine solid electrolytes as well as the composites in Fig. 3(c). By reducing the solid electrolyte volume fraction to 40 and 30 vol %, the activation energy increases. This increase is observed for all three evaluated solid electrolytes in their composites from triplicate measurements [Fig. 3(c)]. The uncertainty of the ionic conductivities is calculated as the standard deviation of the triplicate measurements from one composite per

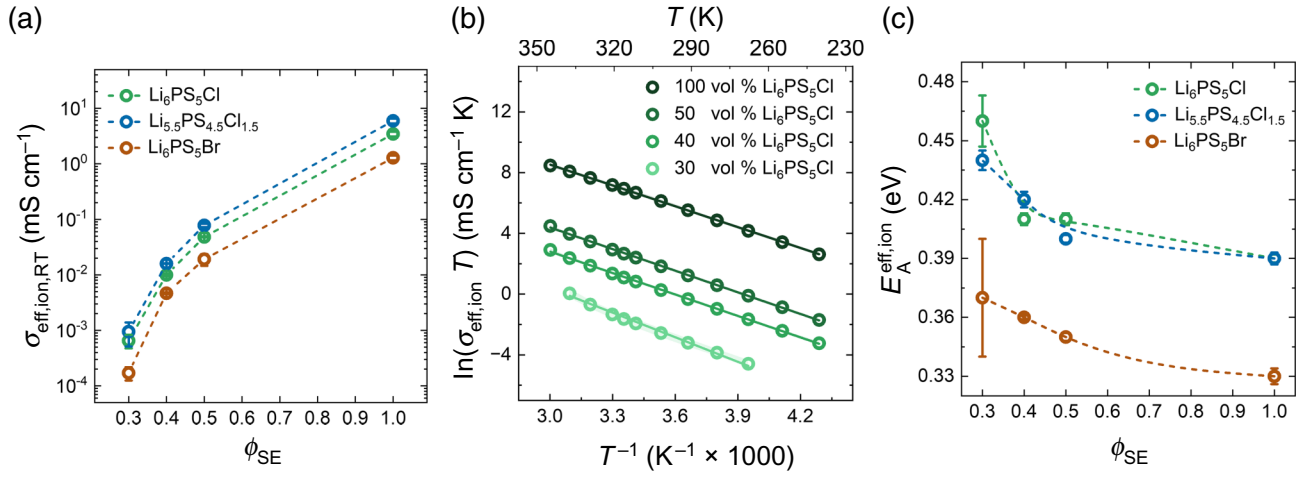

FIG. 3. (a) Effective ionic conductivity at room temperature of all investigated composites, as well as the respective pristine electrolytes versus volume fraction of the solid electrolyte; dashed lines act as guides to the eye. (b) Exemplary Arrhenius plot for the determination of the activation energies of Li_6PS_5Cl composites and pristine electrolyte. (c) Activation energies for all composites and electrolytes versus volume fraction of the solid electrolyte; dashed lines act as guides to the eye.

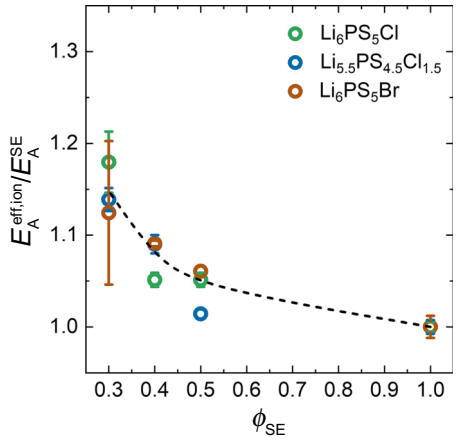

FIG. 4. Normalized activation energies of the composites of all three electrolytes versus volume fraction of the solid electrolyte. Dashed line acts as a guide to the eye.

composition measured in three separate cells; the error of the slope on the resulting Arrhenius plot is used to calculate the uncertainty of the activation energies through error propagation.

A reasonable question to be asked now is whether the relative increase in activation energy of all composites is the same irrespective of the solid electrolyte used. Normalizing the activation energy of each composite ($E_A^{ion,eff}$), as well as that of the pristine electrolytes, by the activation energy of the respective pristine electrolyte (E_A^{SE}) yields the relative activation energies ($E_A^{ion,eff}/E_A^{SE}$) and allows for a direct comparison. Figure 4 shows these normalized activation energies and highlights that the changes in E_A are similar and follow a trend towards higher effective E_A for lower solid electrolyte volume fractions, within the investigated composites. At 30 vol % of the solid electrolyte in the composite, a relative activation energy change of 10% to 20% can be observed. Thus, it is essential to consider the effective ionic transport, especially at low temperatures, when comparing the loading of cells and the performance evaluation of solid-state composites.

One explanation for the increase in activation energy with decreasing solid electrolyte volume fraction could be a constriction resistance effect on the solid-electrolyte–composite interface caused by the reduction in contact area through which lithium transport can occur [36]. Further adding to this hypothesis, temperature-dependent current constriction effects on grain boundaries are possibly contributing to the apparent change in E_A as the quantity of grain boundary interfaces changes [37].

C. Tortuosity factor consideration and impact on solid-state batteries

From the change in normalized activation energy, the commonly used description of the tortuosity factor, κ, to assess information about the microstructural pathways in the composites, can be investigated for its

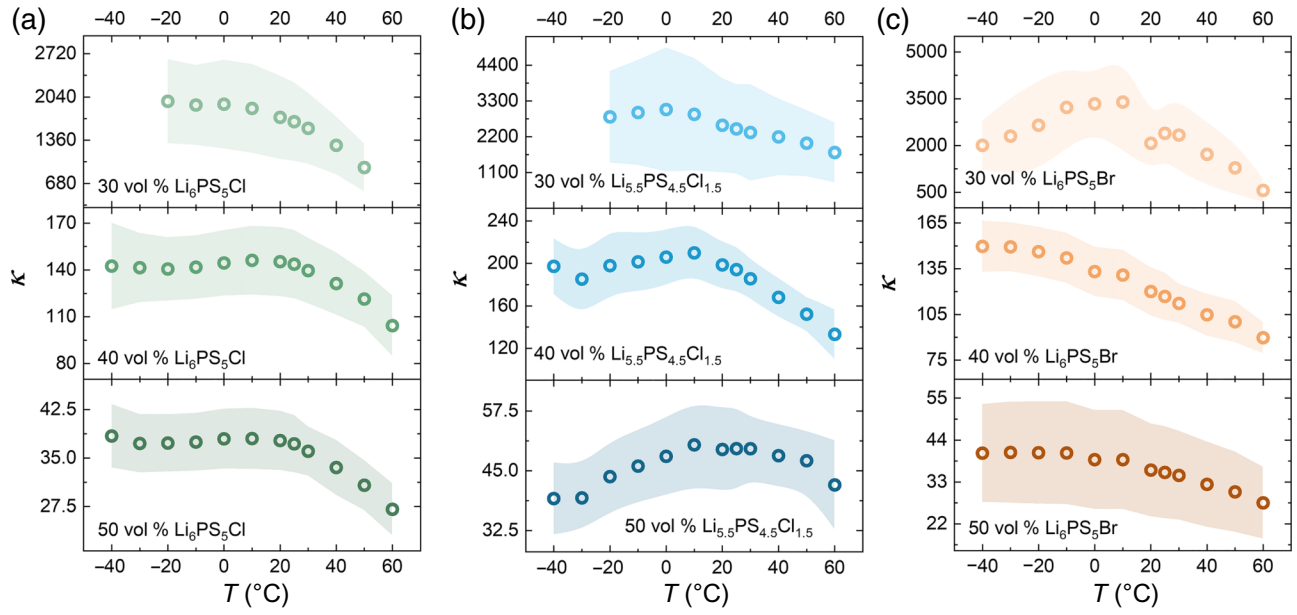

FIG. 5. Tortuosity factor κ at various temperatures for (a) Li_6PS_5Cl in green, (b) $Li_{5.5}PS_{4.5}Cl_{1.5}$ in blue, and (c) Li6PS5Br in brown. κ values and their respective uncertainties through error propagation were calculated using Eq. (1). Temperature dependence is visible. There is no clear trend for low temperatures. However, at temperatures above about 20 °C, there is a visible drop of κ for almost all composites.

temperature dependence [12,15,25,27,38]. The most common approach to calculate the tortuosity factor (κ) is given by

$$\kappa = \phi_{SE}\frac{\sigma_{SE}}{\sigma_{ion,eff}}. \quad (1)$$

The tortuosity factor for solid-state systems is calculated as the product of the volume fraction of the ion conducting phase, ϕ_{SE}, and the ratio of the ionic conductivity of the pristine solid electrolyte, σ_{SE}, and the effective ionic transport of the respective composite, $\sigma_{ion,eff}$. This approach for the determination of the tortuosity factor assumes no temperature dependence. However, as shown in Fig. 3(c), the activation energy changes when the volume ratio of the solid electrolyte to active material is changed, resulting in a temperature dependence of κ. This can be shown by assuming Arrhenius behavior for σ_{SE}:

$$\sigma_{SE} = \frac{\sigma^0_{SE}}{T}\exp\left(-\frac{E^{SE}_A}{k_B T}\right). \quad (2)$$

As Fig. 3(b) shows a linear correlation for the Arrhenius plot [$\ln(\sigma_{ion,eff}\cdot T)$ versus T^{-1}], it can reasonably be assumed that Eq. (3) is true for the systems investigated in this work. Combining Eqs. (1)–(3) and assuming temperature independence for ϕ_{SE}, one can define κ as in Eq. (4). The solid electrolyte volume fractions, ϕ_{SE}, can be assumed to be temperature independent, as the volumetric thermal expansion coefficients of all components are sufficiently small: -8.7×10^{-6} K^{-1} for graphite [39] and 7.8×10^{-6} K^{-1} for silicon [40]. The thermal expansion coefficient of $Li_{5.5}PS_{4.5}Cl_{1.5}$ was assumed to be comparable to that of Li_6PS_5Cl at 66×10^{-6} K^{-1}, and 69×10^{-6} K^{-1} for Li_6PS_5Br, as obtained from Minafra *et al.* [41], suggesting that there is no difference in volume fraction as a function of temperature for all composites:

$$\sigma_{ion,\,eff} = \frac{\sigma^0_{ion,\,eff}}{T}\exp\left(-\frac{E^{ion,\,eff}_A}{k_B T}\right), \quad (3)$$

$$\kappa = \phi_{SE}\frac{\sigma^0_{SE}}{\sigma^0_{ion,\,eff}}\exp\left(\frac{E^{ion,\,eff}_A - E^{SE}_A}{k_B T}\right). \quad (4)$$

This means that if $E^{ion,\,eff}_A \neq E^{SE}_A$ is true, which is the case as per Fig. 4, there needs to be a T dependence of κ. This temperature dependance can be observed in the data: while there is not a clear trend at elevated temperatures (above ~20 °C), there is a visible drop of κ for almost all composites, confirming that $E^{ion,\,eff}_A \neq E^{SE}_A$. Composites with higher amounts of solid electrolyte generally exhibit a smaller change of κ compared to composites with less solid electrolyte, as can be seen in Fig. 5. This means that

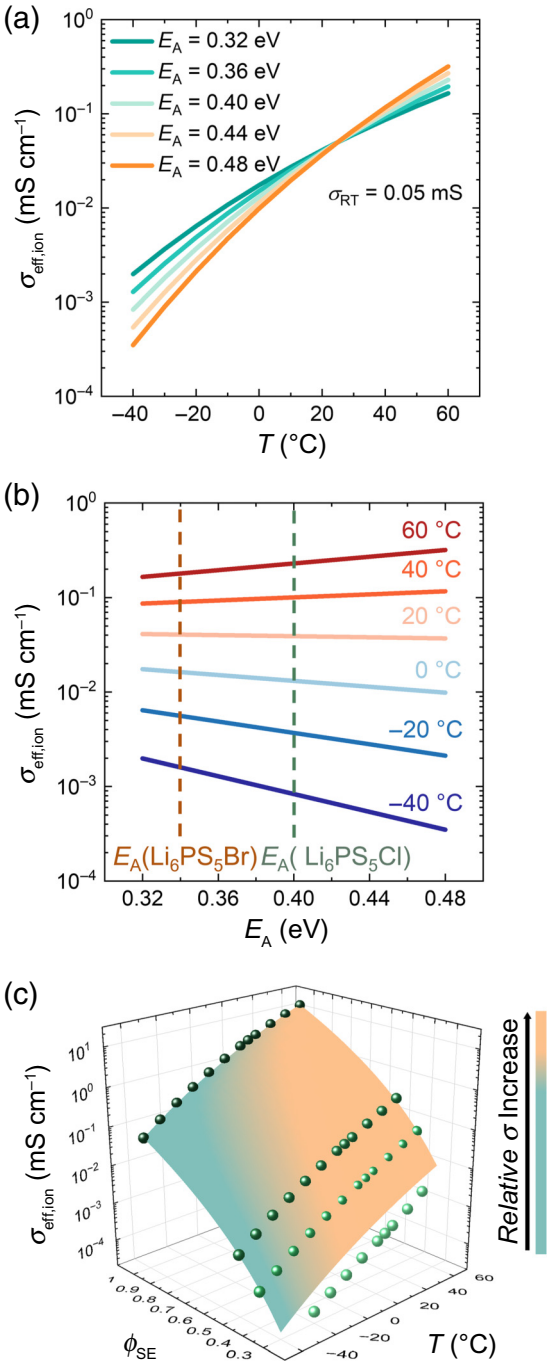

FIG. 6. (a) Calculated effective ionic conductivities with changing activation energy of $E_A(Li_6PS_5Cl)\pm10\%$ and 20% at various temperatures, starting from the activation energy of pristine Li_6PS_5Cl and room-temperature conductivity of the 50 vol % Li_6PS_5Cl composite. (b) Comparison of the isothermal conductivities at five different activation energies; activation energies of Li_6PS_5Cl and Li6PS5Br are highlighted in green and brown, respectively. (c) Three-dimensional representation of Li_6PS_5Cl conductivity in relation to the composite volume ratio and temperature. Hypersurface spanning conductivities calculated from Li_6PS_5Cl conductivities based on a Bruggeman-type fit. Color of the hypersurface shows the relative change in conductivity with temperature for each composition.

the tortuosity factor, κ, needs to be temperature dependent and cannot be a purely geometric factor, highlighting that the tortuosity factor and the geometric tortuosity are not directly related.

This work shows that ionic transport in composites is dependent on temperature and composition, suggesting that, when having more than room-temperature operation as a goal, the transport changes, especially at high active material loadings, need to be considered. To provide an example of how significant a change in ionic transport one would expect upon minor changes in activation energy, Fig. 6(a) shows a theoretical comparison between five different scenarios to show the resulting differences in effective conductivities at high and low temperatures. The activation energy is increased or decreased by 10% and 20%, respectively. As a starting point for the calculation, the room-temperature conductivity of the 50 vol % Li_6PS_5Cl composite, $\sigma = 0.05$ mS cm^{-1}, as well as the activation energy, $E_A = 0.40$ eV, of the pristine electrolyte were chosen. In Fig. 6(a), the respective theoretical conductivities are given as a function of temperature and color graded with respect to the changing activation energies. It becomes obvious that temperature dependences of the effective ionic conductivities are heavily affected by the changing activation energies. This is emphasized even further by noting the absolute values. In Fig. 6(b), isotherms interpolated from this case are given, showing the theoretical effective conductivities resulting at the five activation energies. Even at $T = 0$ °C, the impact of a change in activation energy on the conductivity is already significant, as a 20% increase in activation energy changes the conductivity by nearly 50%. This behavior is accelerated at low temperatures and results in a difference of an order of magnitude at $T = -40$ °C, suggesting electrolytes with low activation barriers—or composites with low active material content—are needed for solid-state batteries that run at lower temperatures. While the low activation barriers being necessary for fast ionic transport at low temperatures seems trivial, the need for a high solid electrolyte content due to the change in activation barriers of the composites is not. In direct contrast to the low-temperature behavior, a higher activation energy may be beneficial for batteries that are operated at elevated temperatures, as the conductivity increases faster with increasing temperature when the activation energy is higher. Figure 6(c) shows the three-dimensional dependency of the experimentally determined conductivities of Li_6PS_5Cl in relation to the composition of the composite and the temperature. The effective ionic transport can be well described by the relatively basic model of the Bruggeman-like effective medium transport combined with the modified Arrhenius behavior found here. It is consequently necessary to take those semiempirical parameters into account while designing temperature-specific solid-state batteries.

IV. CONCLUSION

This work demonstrates how the activation energy of ion transport is affected by the composition of a solid-state electrode composite by utilizing temperature-dependent impedance measurements and transmission line modeling. For three different solid electrolytes (Li_6PS_5Cl, $Li_{5.5}PS_{4.5}Cl_{1.5}$, and Li_6PS_5Br), it was shown that a decrease in the solid electrolyte content in the composite led to an increase in activation energy. These findings and considerations have a direct impact on the application of solid-state batteries. It has been known for a while that for a reasonable loading in solid-state batteries a high ionically conducting electrolyte is needed. This work shows, however, that, besides aiming for a high ionic conductivity at room temperature, the activation energy of the pristine electrolyte also needs to be as low as possible for the operation of solid-state batteries at lower temperatures. Otherwise, the decrease in ionic conductivity may too strongly affect the partial ionic transport in composites. Additionally, by combining the Arrhenius-like description of the temperature dependance with the composition dependance of the ionic conductivity, it was shown that the tortuosity factor, κ, was temperature dependent. Therefore, for fast ionic transport in solid-state electrode composites at low temperatures, low active material loadings are still paramount and more solid electrolyte optimization is clearly needed. It is possible that the influence of electrode composition on the observed activation energy in sulfide-based electrolytes is transferable to other electrolyte systems, such as oxide and polymer-based systems. However, at this stage, it is reasonable to assume that the intensity of the observed trend might differ for other electrolyte systems and different active materials, as the rigidity and particle sizes of the materials used will likely impact on the observed temperature dependence of the effective ionic conductivity. While there has been tremendous progress made in solid-state battery performance at room temperature, the underlying transport characteristics suggest that additional optimization is needed when the operation temperature is changed.

Data that support the findings of this study are made available online through the datastore of the University of Münster [42].

ACKNOWLEDGMENTS

The authors acknowledge financial support within the SilKompAs project funded by the Bundesministerium für Bildung und Forschung (BMBF Project No. 03XP0486B). L.K. acknowledges financial support from the International Graduate School for Battery Chemistry, Characterization, Analysis, Recycling, and Application (BACCARA), which is funded by the Ministry for Culture and Science of North Rhine Westphalia, Germany.

The authors declare no conflicts of interest.

[1] T. Nogueira, E. Sousa, and G. R. Alves, Electric vehicles growth until 2030: Impact on the distribution network power, Energy Rep. **8**, 145 (2022).

[2] Y. G. Cho, M. Li, J. Holoubek, W. Li, Y. Yin, Y. S. Meng, and Z. Chen, Enabling the low-temperature cycling of NMC||graphite pouch cells with an ester-based electrolyte, ACS Energy Lett. **6**, 2016 (2021).

[3] M. A. Kraft, S. P. Culver, M. Calderon, F. Böcher, T. Krauskopf, A. Senyshyn, C. Dietrich, A. Zevalkink, J. Janek, and W. G. Zeier, Influence of lattice polarizability on the ionic conductivity in the lithium superionic argyrodites Li_6PS_5X ($X = $ Cl, Br, I), J. Am. Chem. Soc. **139**, 10909 (2017).

[4] Kang Yan, Jiangyan Wang, Shuoqing Zhao, Dong Zhou, Bing Sun, Yi Cui, and Guoxiu Wang, Temperature-dependent nucleation and growth of dendrite-free lithium metal anodes, Angew. Chem. **131**, 11486 (2019).

[5] J. Janek and W. G. Zeier, Challenges in speeding up solid-state battery development, Nat. Energy **8**, 230 (2023).

[6] Y. Yang, W. Yuan, W. Kang, Y. Ye, Q. Pan, X. Zhang, Y. Ke, C. Wang, Z. Qiu, and Y. Tang, A review on silicon nanowire-based anodes for next-generation high-performance lithium-ion batteries from a material-based perspective, Sustain. Energy Fuels **4**, 1577 (2020).

[7] M. T. McDowell, S. W. Lee, W. D. Nix, and Y. Cui, 25th anniversary article: Understanding the lithiation of silicon and other alloying anodes for lithium-ion batteries, Adv. Mater. **25**, 4966 (2013).

[8] P. Vadhva, A. M. Boyce, A. Hales, M.-C. Pang, A. N. Patel, P. R. Shearing, G. Offer, and A. J. E. Rettie, Towards optimised cell design of thin film silicon-based solid-state batteries via modelling and experimental characterisation, J. Electrochem. Soc. **169**, 100525 (2022).

[9] D. Cao, T. Ji, A. Singh, S. Bak, Y. Du, X. Xiao, H. Xu, J. Zhu, and H. Zhu, Unveiling the mechanical and electrochemical evolution of nano silicon composite anodes in sulfide based all-solid-state batteries, Adv. Energy Mater. **13**, 2203969 (2023).

[10] Y. Rudel, M. Rana, J. Ruhl, C. Rosenbach, J. Müller, P. Michalowski, A. Kwade, and W. G. Zeier, Investigating the influence of the effective ionic transport on the electrochemical performance of Si/C-argyrodite solid-state composites, Batter. Supercaps **6**, e202300211 (2023).

[11] M. Rana, Y. Rudel, P. Heuer, E. Schlautmann, C. Rosenbach, M. Y. Ali, H. Wiggers, A. Bielefeld, and W. G. Zeier, Toward achieving high areal capacity in silicon-based solid-state battery anodes: What influences the rate-performance? ACS Energy Lett. **8**, 3196 (2023).

[12] Y. Kato, S. Shiotani, K. Morita, K. Suzuki, M. Hirayama, and R. Kanno, All-solid-state batteries with thick electrode configurations, J. Phys. Chem. Lett. **9**, 607 (2018).

[13] L. Peng, C. Yu, Z. Zhang, H. Ren, J. Zhang, Z. He, M. Yu, L. Zhang, S. Cheng, and J. Xie, Chlorine-rich lithium argyrodite enabling solid-state batteries with capabilities of high voltage, high rate, low-temperature and ultralong cyclability, Chem. Eng. J. **430**, 132896 (2022).

[14] P. Lu, *et al.*, Rate-limiting mechanism of all-solid-state battery unravelled by low-temperature test-analysis flow, Energy Storage Mater. **67**, 103316 (2024).

[15] G. F. Dewald, S. Ohno, J. G. C. Hering, J. Janek, and W. G. Zeier, Analysis of charge carrier transport toward optimized cathode composites for all-solid-state Li − S batteries, Batter. Supercaps **4**, 183 (2021).

[16] P. Minnmann, L. Quillman, S. Burkhardt, F. H. Richter, and J. Janek, Editors' choice—quantifying the impact of charge transport bottlenecks in composite cathodes of all-solid-state batteries, J. Electrochem. Soc. **168**, 040537 (2021).

[17] T. A. Hendriks, M. A. Lange, E. M. Kiens, C. Baeumer, and W. G. Zeier, Balancing partial ionic and electronic transport for optimized cathode utilization of high-voltage $LiMn_2O_4/Li_3InCl_6$ solid-state batteries, Batter. Supercaps **6**, e202200544 (2023).

[18] W. Zhang, *et al.*, Interfacial processes and influence of composite cathode microstructure controlling the performance of all-solid-state lithium batteries, ACS Appl. Mater. Interfaces **9**, 17835 (2017).

[19] K. G. Naik, B. S. Vishnugopi, and P. P. Mukherjee, Kinetics or transport: Whither goes the solid-state battery cathode? ACS Appl. Mater. Interfaces **14**, 29754 (2022).

[20] J. Zahnow, T. Bernges, A. Wagner, N. Bohn, J. R. Binder, W. G. Zeier, M. T. Elm, and J. Janek, Impedance analysis of NCM cathode materials: Electronic and ionic partial conductivities and the influence of microstructure, ACS Appl. Energy Mater. **4**, 1335 (2021).

[21] See the Supplemental Material at http://link.aps.org/supplemental/10.1103/PRXEnergy.3.033004 for a Pawley fit of the x-ray diffraction patterns of the solid electrolytes. Furthermore, the volume and mass ratios for all composites are given. The temperature-dependent impedance spectra of all pristine electrolytes with the corresponding equivalent circuits as well as the cell setup are given. The confirmation of the TLM with data gathered from direct current measurements, as well as an exemplary fit of low-temperature impedance spectra, including the high-frequency process for pristine Li_6PS_5Cl and the 50 vol % Li_6PS_5Cl composite, and the equivalent circuit used to fit the 50 vol % SE composite, are provided as well. Additionally, all temperature-dependent impedance spectra of all composites, together with the respective fits and the resulting conductivities, are also shown, and the Arrhenius plots for $Li_{5.5}PS_{4.5}Cl_{1.5}$ and Li_6PS_5Br are given. It also contains Refs. [17,25].

[22] J. Müller, *et al.*, Si-on-graphite fabricated by fluidized bed process for high-capacity anodes of Li-ion batteries, Chem. Eng. J. **407**, 126603 (2021).

[23] R. Koerver, W. Zhang, L. De Biasi, S. Schweidler, A. O. Kondrakov, S. Kolling, T. Brezesinski, P. Hartmann, W. G. Zeier, and J. Janek, Chemo-mechanical expansion of lithium electrode materials-on the route to mechanically optimized all-solid-state batteries, Energy Environ. Sci. **11**, 2142 (2018).

[24] E. Schlautmann, *et al.*, Impact of the solid electrolyte particle size distribution in sulfide-based solid-state battery composites, Adv. Energy Mater. **13**, 2302309 (2023).

[25] S. Ohno, C. Rosenbach, G. F. Dewald, J. Janek, and W. G. Zeier, Linking solid electrolyte degradation to charge carrier Transport in the thiophosphate-based composite cathode toward solid-state lithium-sulfur batteries, Adv. Funct. Mater. **31**, 2010620 (2021).

[26] C. König, V. Miß, L. Janin, and B. Roling, Mitigating the ion transport tortuosity in composite cathodes of all-solid-state batteries by wet milling of the solid electrolyte particles, ACS Appl. Energy Mater. **6**, 9356 (2023).
[27] J. Landesfeind, J. Hattendorff, A. Ehrl, W. A. Wall, and H. A. Gasteiger, Tortuosity determination of battery electrodes and separators by impedance spectroscopy, J. Electrochem. Soc. **163**, A1373 (2016).
[28] M. Cronau, A. Paulus, L. P. Pescara, M. Kroll, D. Renz, J. A. Mekontso, A. Marx, and B. Roling, What limits the rate capability of ultrathick composite electrodes in lithium-ion batteries? A case study on the thickness-dependent impedance of $LiCoO_2$ cathodes, Batter. Supercaps **5**, e202200194 (2022).
[29] A. Weber and S. Dierickx, From microstructure to performance: A detailed multi-level study of SOFC anodes, ECS Trans. **91**, 1827 (2019).
[30] S. Dierickx, T. Mundloch, A. Weber, and E. Ivers-Tiffée, Advanced impedance model for double-layered solid oxide fuel cell cermet anodes, J. Power Sources **415**, 69 (2019).
[31] I. M. Hodge, M. D. Ingram, and A. R. West, Impedance and modulus spectroscopy of polycrystalline solid electrolytes, J. Electroanal. Chem. **74**, 125 (1976).
[32] J. T. S. Irvine, D. C. Sinclair, and A. R. West, Electroceramics: Characterization by impedance spectroscopy, Adv. Mater. **2**, 132 (1990).
[33] Y. Liu, Y. Bai, W. Jaegermann, R. Hausbrand, and B. X. Xu, Impedance modeling of solid-state electrolytes: Influence of the contacted space charge layer, ACS Appl. Mater. Interfaces **13**, 5895 (2021).
[34] A. E. Bumberger, A. Nenning, and J. Fleig, Transmission line revisited – the impedance of mixed ionic and electronic conductors, Phys. Chem. Chem. Phys. **26**, 15068 (2024).
[35] T. Böger, T. Bernges, Y. Li, P. Canepa, and W. G. Zeier, Thermal conductivities of lithium-ion-conducting solid electrolytes, ACS Appl. Energy Mater. **6**, 10704 (2023).
[36] J. K. Eckhardt, P. J. Klar, J. Janek, and C. Heiliger, Interplay of dynamic constriction and interface morphology between reversible metal anode and solid electrolyte in solid state batteries, ACS Appl. Mater. Interfaces **14**, 35545 (2022).
[37] J. K. Eckhardt, S. Kremer, T. Fuchs, P. Minnmann, J. Schubert, S. Burkhardt, M. T. Elm, P. J. Klar, C. Heiliger, and J. Janek, Influence of microstructure on the material properties of LLZO ceramics derived by impedance spectroscopy and brick layer model analysis, ACS Appl. Mater. Interfaces **15**, 47260 (2023).
[38] I. V. Thorat, D. E. Stephenson, N. A. Zacharias, K. Zaghib, J. N. Harb, and D. R. Wheeler, Quantifying tortuosity in porous Li-ion battery materials, J. Power Sources **188**, 592 (2009).
[39] M. A. Abdullah, T. M. B. Albarody, and A. R. Hussein, Graphite thermal expansion coefficient measured by *in-situ* x-ray diffraction, Nanotechnology **31**, 285709 (2020).
[40] W. M. Yim and R. J. Paff, Thermal expansion of AlN, sapphire, and silicon, J. Appl. Phys. **45**, 1456 (1974).
[41] N. Minafra, M. A. Kraft, T. Bernges, C. Li, R. Schlem, B. J. Morgan, and W. G. Zeier, Local charge inhomogeneity and lithium distribution in the superionic argyrodites Li_6PS_5X ($X = $ Cl, Br, I), Inorg. Chem. **59**, 11009 (2020).
[42] https://doi.org/10.17879/16958461473